

Dynamic Features of Flare Plasma Unveiled with Recent Observations

Ayumi Asai

*Unit of Synergetic Studies for Space, Kyoto University
Yamashina, Kyoto, 607-8471, Kyoto*

Abstract. Solar flares are very spectacular, and they are accompanied by a variety of plasma motions. As a flare evolves, flare loops show many dynamic features of plasma, such as, flare plasma heating and cooling, chromospheric evaporation, reconnection inflow and outflow, and so on. In addition, many ejection phenomena, such as filament/prominence eruptions have been observed in the chromospheric lines, in the extreme ultraviolet (EUV), and in X-rays. Flare-associated waves and the related plasma motions have also been studied. These plasma motions can be observed as phenomena accompanied by Doppler shifts in spectroscopic observations. Therefore, spectroscopic observations are crucially important for understanding the dynamics of flare plasma. Moreover, with multi-wavelength observations, we synergistically understand the flare physics in morphologically, qualitatively, and quantitatively. We overview recent observations of solar flares especially done by *Hinode*, STEREO, and SDO, and show (only a small part of) the dynamic features of flare plasma.

1. Plasma Flows in Magnetic Reconnection

Solar flares are really spectacular. After the first observation 150 years ago (Carrington 1859), solar flares have been extensively observed in various wavelengths. As a comprehensive view of solar flares, the magnetic reconnection model proposed by Carmichael (1964); Sturrock (1966); Hirayama (1974); Kopp & Pneuman (1976) (the CSHKP model) has been widely discussed. The CSHKP model suggests that magnetic field lines successively reconnect in the corona, and it can explain several well-known features of solar flares. Around the reconnection region, reconnection inflow (plasma flow toward the current sheet) and outflow (plasma flow outward from the current sheet) must occur. In a macroscopic view, the reconnection outflows are observed as ejections of plasmoids/filaments. Beneath the reconnection regions, on the other hand, we observed post-flare loops and formation of the $H\alpha$ two-ribbon structures at their footpoints. Associated with flare, coronal disturbances and wave-like features are also observed. In Figure 1 we present a cartoon of the magnetic reconnection model.

To understand these dynamic features, spectroscopic observations are crucially required. On the other hand, the apparent plasma motions by filtergram observations are also important. After the launch of *Hinode* in 2006, the sun had an extremely long and deep solar minimum. There have been a very few large flares observed by *Hinode*, and therefore, we are still waiting other large flares. However, it is certainly true that new instruments for solar observations are providing us a new insight on solar flares and magnetic reconnection there. Here, we overview recent works on solar flares and

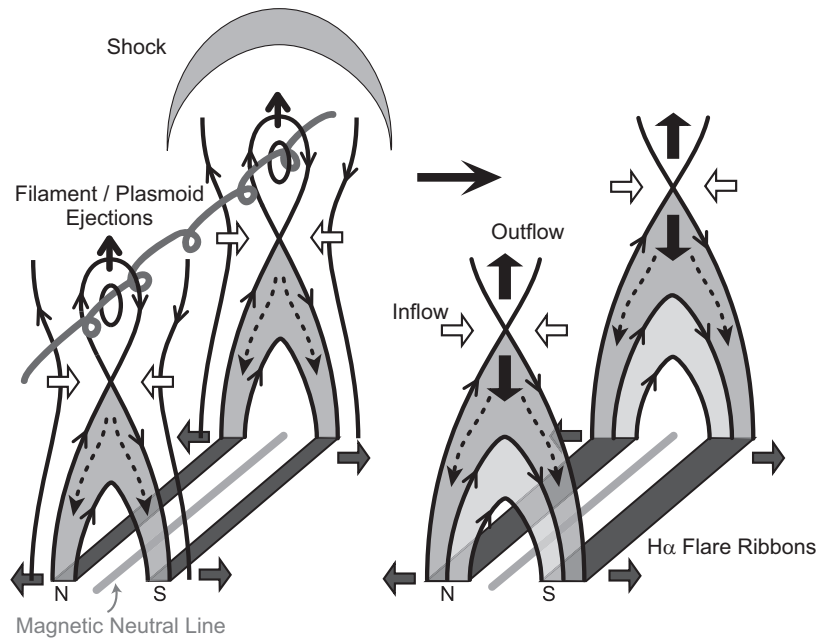


Figure 1. Cartoon of magnetic reconnection. Solid lines show the magnetic field lines. N/S show the magnetic polarities of the positive/negative. Reconnected magnetic field lines form post-flare loops with a cusp-shaped structure. At the footpoints of the post-flare loops the $H\alpha$ flare ribbons are generated due to the precipitation of nonthermal particles and thermal conduction into the chromosphere. At the front of filament/plasmoid ejections, shocks are formed (Asai et al. 2004a).

review the dynamic features unveiled with recent observations especially by *Hinode*, STEREO, and SDO.

2. Inflows

After the first report of the observation on the reconnection inflow in the corona by Yokoyama et al. (2001) (Fig. 2), inflow features have been extensively observed and studied, since they are a direct and straightforward evidence of the magnetic reconnection. Yokoyama et al. (2001) reported that the apparent inflow velocity V_{in} of EUV-emitting plasma seen in SOHO/EIT images is about 5 km/s, which corresponds to the reconnection rate ($= V_{in}/V_A$; coronal Alfvén Mach number) of about 0.001 – 0.03. Furthermore, Narukage & Shibata (2006) statistically analyzed the apparent inflows by using SOHO/EIT data, and confirmed that V_{in} is about 2 – 14 km/s, which corresponds to the reconnection rate of about 0.001 – 0.07. SDO has also observed many inflows with the velocity of a few tens of km/s. With the higher temporal and spatial resolutions, the more detailed properties of reconnection inflows will be cleared.

Lin et al. (2005) showed a beautiful result on the spectral properties of reconnection inflow, by using SOHO/UVCS data. We found two bright features in the $Ly\alpha$ line that are located on both sides of the current sheet and are approaching to each other with the velocity of about several tens of km/s. Moreover, the bright pairs also show the Doppler shift in the UVCS spectral data, with the velocity of about a few tens of

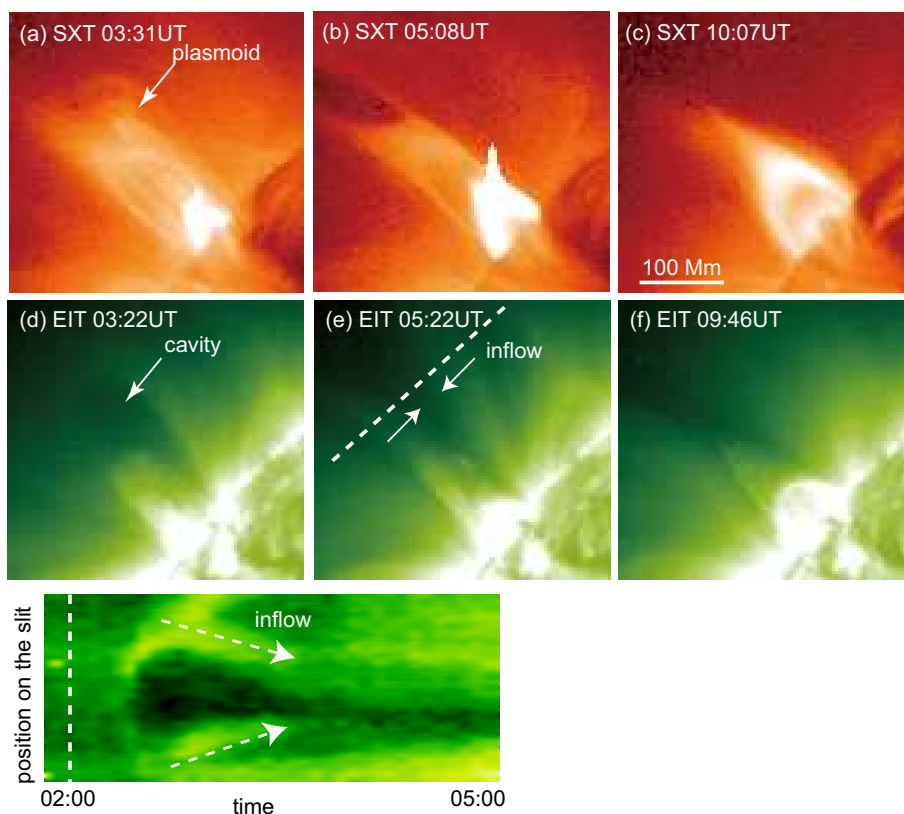


Figure 2. Time evolution of a reconnection inflow. Soft X-ray images (a, b, and c) and EUV ($\text{Fe } 195 \text{ \AA}$) images (d, e, and f) are taken by *Yohkoh*/SXT and by SOHO/EIT, respectively. The bottom left panel shows the evolution of the one-dimensional plot of EIT data (in the negative image) nearly along the dashed line in the panel (e). *Courtesy of T. Yokoyama and H. Isobe.*

km/s. These imply the reconnection rate of about 0.01. These values of the reconnection rate (0.001 – 0.03) means that the magnetic reconnection at solar flares is much faster than the steady reconnection by the Sweet-Parker model (Sweet 1958; Parker 1957) that predicts the reconnection rate of about 10^{-7} .

3. Outflows, Plasmoid Ejections, and Downflows

To understand detailed properties of reconnection outflow is also crucially important for magnetic reconnection theories, since dynamic features inside the current sheet are still invisible in solar flares and firstly appear as reconnection outflows. The bidirectional flow reported by Innes et al. (1997) was one of the most sensational results as the observation on the reconnection outflow. Associated with explosive events, the bidirectional flow with the velocity of about 100 km/s is observed by SOHO/SUMER. Such bidirectional flows have been also observed by SOHO/CDS and *Hinode*/EIS. Wang et al. (2007) reported an example of the direct spectroscopic observation on the reconnection outflow (Fig. 3). They found enhanced blue-side tails in line profiles of Fe XIX (8 MK)

well above the flare loops. The line-of-sight velocity is about 600 km/s, and even higher velocity of about 1800 – 3500 km/s is expected if the projection effect is corrected.

By *Hinode*/EIS, similar fast flows above flare loops have been also reported. Hara et al. (2009) found a brightening in a flare line (Fe xxiii; 263.7 Å) at the top of a flare loop. They also found a hot outflow (upward flow) from the loop top hot region with the Doppler velocity of about 200 – 400 km/s in the Ca xvii line (192.86 Å). In the cooler lines, on the other hand, a flow toward the hot region is also identified. These are suggested to be the reconnection outflow and inflow, respectively.

In a macroscopic view, (upward) reconnection outflows are observed as plasmoid/filament ejections. They start to rise up slowly (with the velocity of several km/s) before the main phase of a flare, and are accelerated during the impulsive phase. The final velocity (near the solar surface) is typically about a few hundred of km/s, which is even smaller than the Alfvén velocity in the corona. Ohyama & Shibata (1998) clearly showed that the ejecta are strongly accelerated during the hard X-ray (HXR) burst. HXR emissions are mainly from energetic electrons precipitating into the chromosphere, and therefore, we expect strong energy release during the HXR burst. The correlation between the plasmoid ejection and HXR emission indicates that plasmoid ejections are strongly related with the energy release (magnetic reconnection process). In other words, ejections regulate the speed of magnetic reconnection. This is easily understood in qualitatively. Fast plasmoid ejection induces thinning of the current sheet beneath the plasmoid because of the mass conservation, which also induces fast reconnection inflow. This has been discussed as a modified model of magnetic reconnection (“plasmoid-induced-reconnection”, Shibata 1996, 1997).

Here, we mention more about the quantitative properties of plasmoid ejections. Ejected plasmoid sometimes shows sub-structure in it. A plasmoid ejection seems to be an ensemble of small plasmoids. Nishizuka et al. (2010) showed an example of such “multiple plasmoid ejection”. Similarly, Karlický et al. (2002) reported that drifting radio signature associated with plasmoid ejection also show the sub-structure in it. From the recent results of numerical simulation on magnetic reconnection, the formation of many tiny islands is expected inside the current sheet (e.g. Shibata & Tanuma 2001). They are ejected from the X-point, and sometimes coalesce into larger islands. Therefore, the sub-structure of plasmoids could be each of such small magnetic islands. Interestingly, the timing of each small plasmoid ejection corresponds to a sub-peak of HXR emission. This result again supports that plasmoid ejection regulates the magnetic reconnection process. Moreover, these fractal features of plasmoids probably enhance magnetic reconnection rate effectively in flares, and have been paid attention to.

With the progress of recent instruments for solar observations, such as by SDO, we can obtain the higher spatial and temporal resolution images for plasmoid ejections. They have revealed the finer structures in plasmoid ejections. The right panels of Figure 4 shows the evolution of the visible current sheet structure observed by SDO in 193 Å associated with an over-the-limb flare that occurred on 2010 August 18. The dark regions in the left-hand side are the solar disk, and bright thin structure is the current sheet. Blobs (plasmoids) in the current sheet are ejected in both direction (sunward and outward) with the velocity of about 200 km/s. We can also see coalescence of blobs.

Sun-ward dark (sometimes bright) features have been observed far above post-flare loops after the main phase of a flare. McKenzie & Hudson (1999) first reported such “downflow”, or sometimes called tadpole structure, in soft X-ray images by *Yohkoh*/SXT.

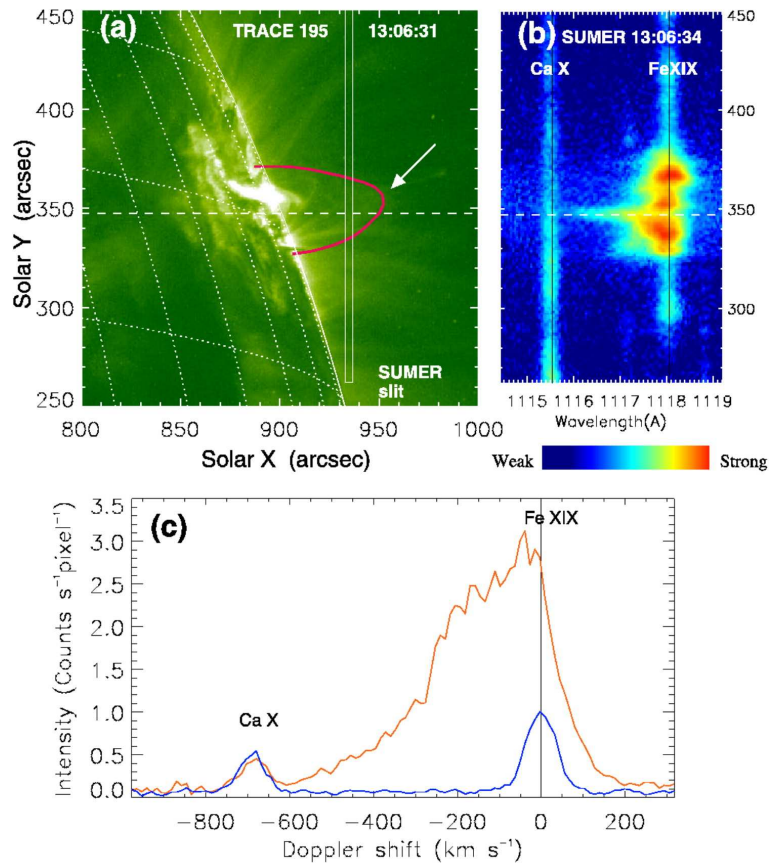


Figure 3. Observations of a high-speed plasma outflow. (a) TRACE 195 Å image showing the compact flare loop. A sketch of the faint, rising loop (red curve) is indicated to show its spatial relation to the SUMER slit. (b) SUMER spectra along the slit in a window containing lines, Ca x (557.7 Å) and Fe xix (1118.1 Å). (c) The spectral line profiles of Fe xix (red curve) along the dashed line in panel (b). The blue curve is the Fe xix line profile taken about a half hour before the event, showing the stationary profile (Wang et al. 2007). Copyright held by AAS.

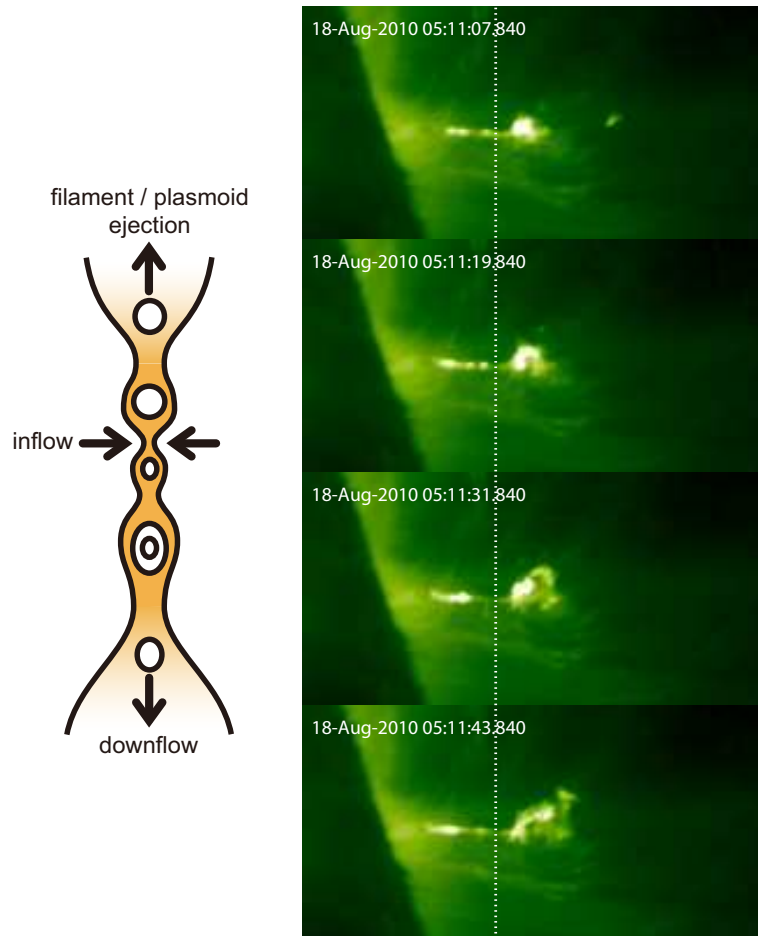


Figure 4. *Left:* Cartoon of the plasmoid formation in a current sheet. *Right:* Time evolution of EUV images by SDO (193 Å). The bright current sheet appears for several minutes and tiny blobs are ejected in both directions in it. *Courtesy of S. Takasao.*

Such downflow motions have been also seen by EUV imaging data. The background faint regions is filled with superhot plasma of supra-arcade with the temperature of about 20 MK. The downflow features are thought to be hotter and less dense than the ambient plasma (McKenzie 2000; Innes et al. 2003). In these phases (main and decay phases) of a flare, the reconnection point is located high in the corona, and downflows are thought to be related with the downward reconnection outflow as we see in Figure 4.

Asai et al. (2004b), moreover, showed that the timing of each downflow seen in EUV (195 Å) images taken by TRACE corresponds to sub-peaks of HXR emission like as for plasmoid ejections (Fig. 5). This again strongly supports that the downflow features are related with the downward reconnection outflow. Furthermore, Innes et al. (2003) showed the spectral features by using the SOHO/SUMER data. Although the observing windows for the emission lines are limited, the red-wing of the Fe XII line (1349 Å) is enhanced. If this enhancement is caused by the Fe XXI line (1354 Å), which is located next to the Fe XII, it must have a blue-ward velocity of about 1000 km/s. The

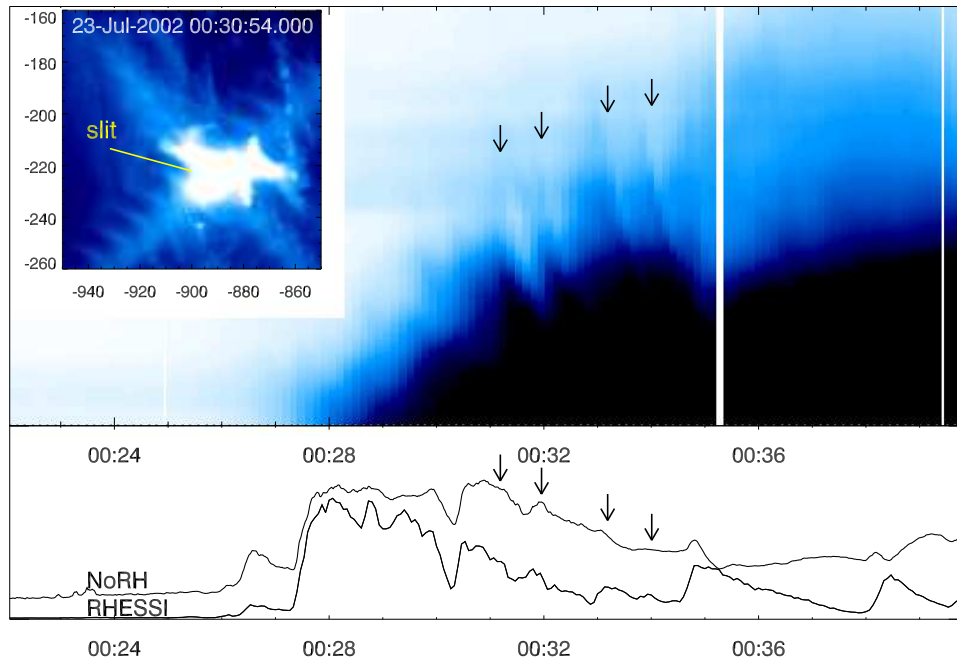


Figure 5. Time evolution of EUV images by TRACE (195 Å) (top right) along the slit line shown in line shown in the top left panel in the negative image. The plots in the bottom panel are microwave (17 GHz) and HXR (50 – 100 keV) light curves with NoRH and RHESSI, respectively (Asai et al. 2004b).

regions of such red-enhancement of the Fe xii lines are associated with the regions of downflows.

4. Shocks and Coronal Disturbances

Associated with large flares and/or fast coronal mass ejections (CMEs), MHD shocks are expected to be formed at the front of an ejection (Fig. 1). Shocks travel in the corona and in the interplanetary space, accelerating particles. They are often observed as type-II radio bursts (or interplanetary type-II radio bursts). Such shocks are also very important for space weather researches, since they could be an effective factor to generate solar energetic particles.

Moreton waves are faint phenomena seen in $H\alpha$ images associated with flares (Moreton 1960). They have quite narrow opening angles and travel in the specific directions that are the same as those of filament eruptions. The traveling speed is as fast as about 1000 km/s, which is much faster than the fast-mode shock speed in the chromosphere. Uchida (1968) suggested the theoretical model for Moreton waves that they are the intersections of MHD fast-mode shock that are traveling in the corona with the chromosphere. *Yohkoh*/SXT also observed faint wave-like phenomena, and are called “X-ray wave” (Khan & Aurass 2002). Narukage et al. (2002), furthermore, found an example of the simultaneous observation of Moreton wave and X-ray wave. Their properties correspond well to each other, and therefore, X-ray waves are thought to be the coronal counterpart of Moreton waves.

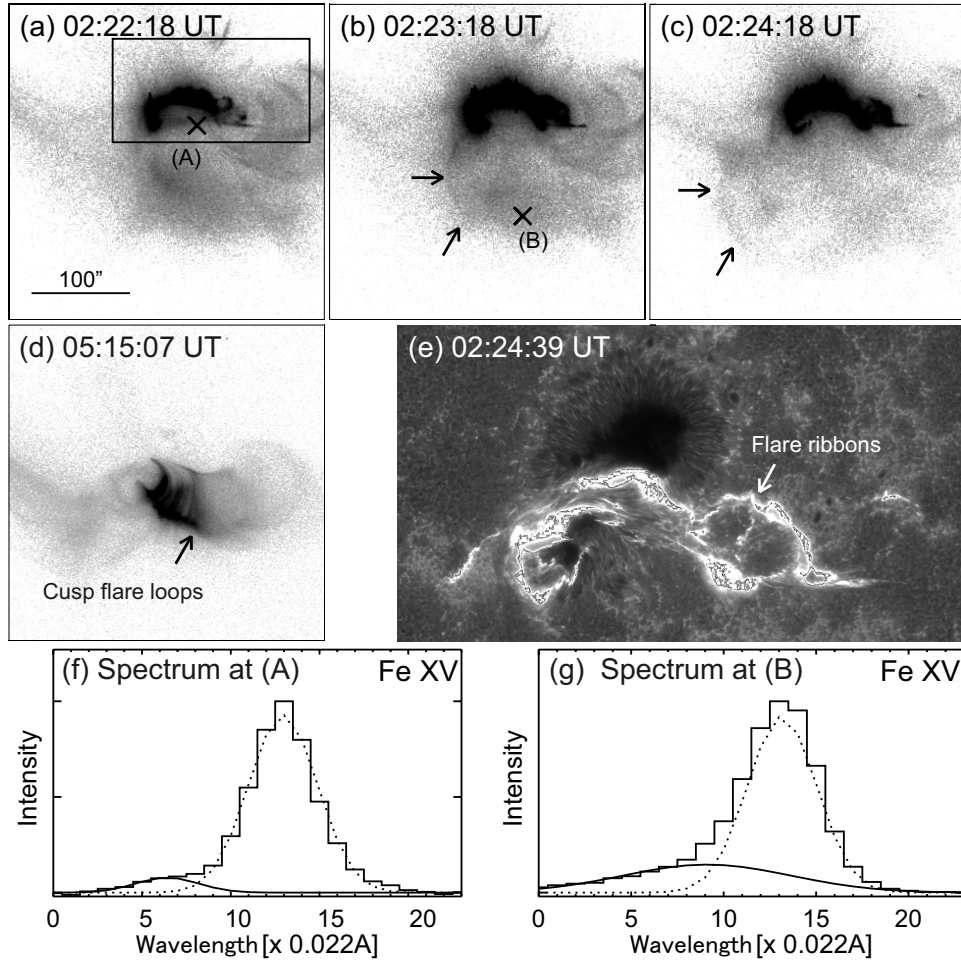


Figure 6. (a ~ d) Soft X-ray negative images taken with the Hinode XRT. The arrows of panels (b) and (c) show the front of the wavelike ejection. (e) Ca II H-line image taken by *Hinode*/SOT. The FOV is shown by the box in panel (a). (f and g) Normalized spectra at the crosses (×) of (A) and (B) in Fe XV window. The solid histograms show the spectra, and the dotted and solid black lines are the fitting results that represent the main and the blueshift components of the line (Asai et al. 2008).

Hinode/XRT observed an X-ray wave associated with the typical two-ribbon flare on 2006 December 13 as we show in Figure 6. The wave-like faint feature shown in the Figure 6(a, b, and c) has a velocity of about 600 km/s in the plane of the sky. The feature also crossed the *Hinode*/EIS slit. We compared the spectral features of a X-ray emitting plasmoid ejection (A) with that of an X-ray wave (B) in Figures 6(f) and (g), respectively. The spectral features are very different to each other. The blueshifted component of the X-ray wave shows the very wide spectra, and is seen only in hotter lines (Fe xv and Ca xvii) used for the observation, while the blueshifted component for the plasmoid ejection (panel f) is not so wide and is seen all the lines used for the observation. This means that there is a strong velocity field of hot plasma with the temperature of 2 MK and more along the line of sight for the X-ray wave. An expanding shell associated with a shock front, for example, can explain the properties of the spectra. From the XRT and EIS observations, the Alfvén Mach number is expected to be about 1.4 for these wave phenomena (N. Narukage, in private communications).

EIT waves (Thompson et al. 2000) are another interesting topic for coronal disturbances. After the launch of the SOHO satellite, EIT have observed the coronal disturbances much more frequently. They are expected to be the coronal counterpart of Moreton waves. On the other hand, their physical properties are much different from those of Moreton waves/X-ray waves. The traveling speed is typically about 300 km/s, and is about one-third of that for Moreton waves. They are traveling isotropically, that is with very wide opening angle, from flare sites. Therefore, EIT waves are not the direct counterpart of Moreton waves. Chen et al. (2002) suggested in their numerical simulation that Moreton waves/X-ray waves are the legs of piston-driven shock formed in the corona and EIT waves are associated with plasma enhancement generated behind the shock.

On the other hand, EUV images taken by recent instruments of STEREO and SDO have given us new aspects of EIT waves (we should rename as EUV waves). Figure 7 shows an example of coronal disturbances associated with the 2010 February 7 flare. The EUV images (195 Å) taken by STEREO/EUVI show both the Moreton wave-like and the EIT wave-like features simultaneously. $H\alpha$ and soft X-ray images of this flare are obtained by ground-based observations (NAOJ-Mitaka and Hida Observatory, Kyoto University) and by *Hinode*/XRT, respectively. The $H\alpha$ images clearly shows Moreton wave traveling with the velocity of about 800 km/s in the south-east direction. The XRT images also shows a faint wave-like feature. We compared the front positions of the sharp and fast traveling disturbances (pointed by the red arrows in Fig. 7) and confirmed that they are well correlated with the fronts of the $H\alpha$ Moreton wave/X-ray wave. The EUV images by SOHO/EIT did not show these front but typical EIT wave traveling with the velocity of about 250 km/s in much wider direction than that for the Moreton wave. The positions of the EIT wave fronts are consistent with those of faint disturbance observed by STEREO/EUVI (shown with the green arrows in Fig. 7).

We, moreover, confirmed that the Moreton wave and the X-ray wave are very transient and are observed only for 5 minutes just after the start of the flare. Then, the front quickly gets fuzzy and is merged with that of the EIT wave. These also support that the Moreton/X-ray waves are the legs of the piston-driven shock formed in the front of the ejecta, and the EIT wave is from another origin.

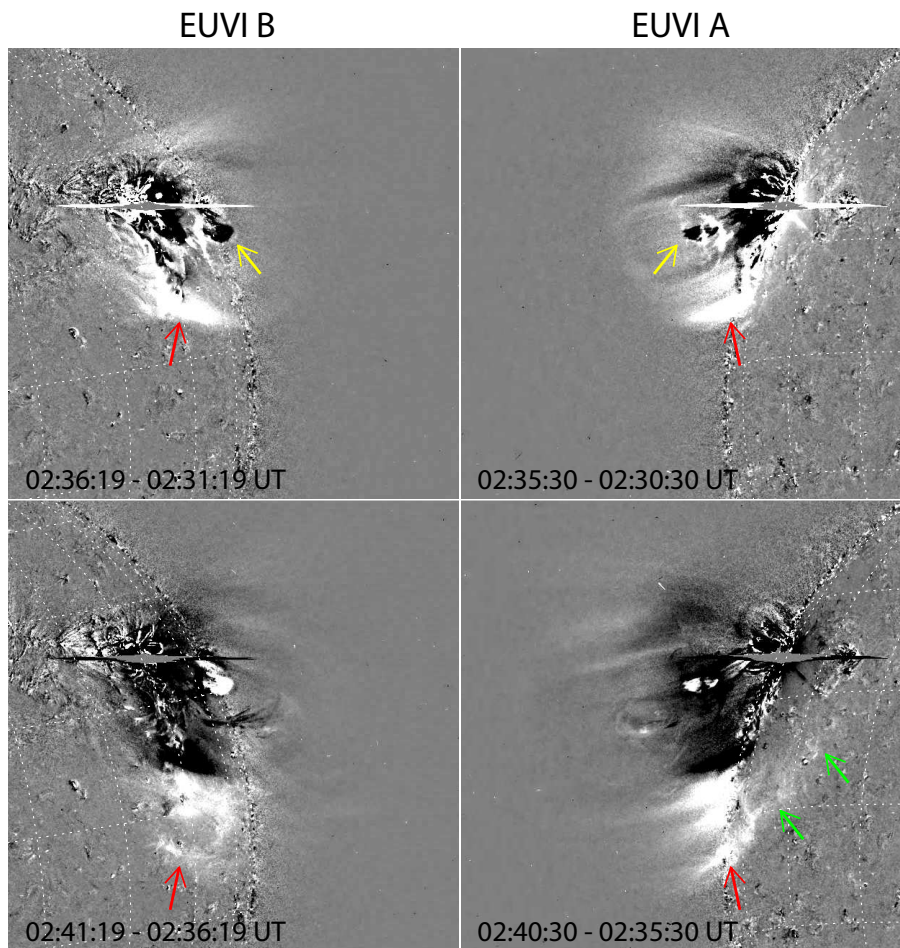


Figure 7. Time evolution of EUV images (195 \AA) by STEREO-B/EUVI (*left*) and STEREO-A/EUVI (*right*). All are the running-difference images. The yellow arrows point the ejection. The red and green arrows show the fronts of the sharp and fast (Moreton wave-like) disturbance and those of the EIT wave-like feature, respectively.

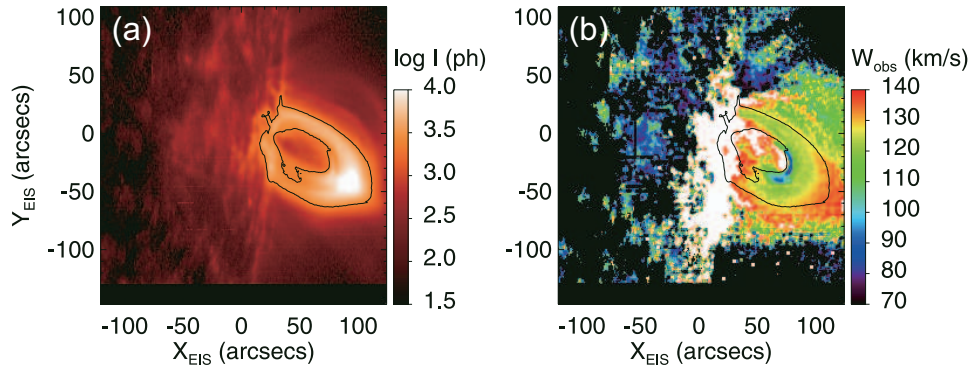


Figure 8. Spectral features of the 2006 December 17 flare derived from *Hinode*/EIS. (a) Ca xvii (192 Å) intensity map from which the Fe xi contribution is subtracted. (b) FWHM map of Ca xvii line. (Hara et al. 2008).

5. Flare Loops, Ribbons/Kernels

As the final topic of the dynamic features of solar flares, we discuss flare loops and flare ribbons here. Explosive upflow at footpoints of flare loops occurs due to the energy input by thermal conduction and/or bombardment of nonthermal plasma. The upflow is called “chromospheric evaporation” (Hirayama 1974; Antonucci et al. 1984, see also Fig. 1).

The evaporated plasma quickly fills the flaring loops, and the loops are illuminated such as in X-rays. *Hinode*/EIS successfully observed post-flare loops of a long-duration event in many EUV emission lines, in the 2006 December 17 flare (Fig. 8). Hara et al. (2008) found the nonthermal broadening of the emission line at the loop top cusps. The used emission line was Ca xvii (192 Å), and the effective temperature is quite high of about 5 MK. These cusp regions are located just beneath the X-point, and therefore, are expected to contain reconnection outflows and/or interactions with closed loops. The observed broadening of the hot line at the cusp region could be caused under such very turbulent conditions. As I already showed, generations and ejections of tiny plasmoids could also cause such broadenings, although more detailed informations for this region are required.

Hara et al. (2008) also reported that post-flare loop structure is seen in all of the emission lines used for the observation. However, the size and the position/shape of the illuminated loops are slightly different to each other. The cooler loops are located more inner part than the hotter line loops. This supports the magnetic reconnection model, since it expects that the newly reconnected loops are located the outermost side, and therefore, the hottest loops should be located at the outermost part (Fig. 1).

At footpoints of flaring loops, on the other hand, strong upflows of hot plasma associated with the chromospheric evaporation and downward motion of chromospheric plasma as the counter-reaction (so-called, “red-asymmetry” of chromospheric lines (e.g. Ichimoto & Kurokawa 1984)). There have been many studies on the evaporation flows with spectroscopic observations with SOHO/CDS or *Hinode*/EIS (e.g. Milligan & Dennis 2009, Fig. 9). Milligan & Dennis (2009) especially compared the chromospheric evaporation with HXR emissions by the RHESSI hard X-ray data. They clearly showed temperature-depending upflows at the HXR-emitting footpoints.

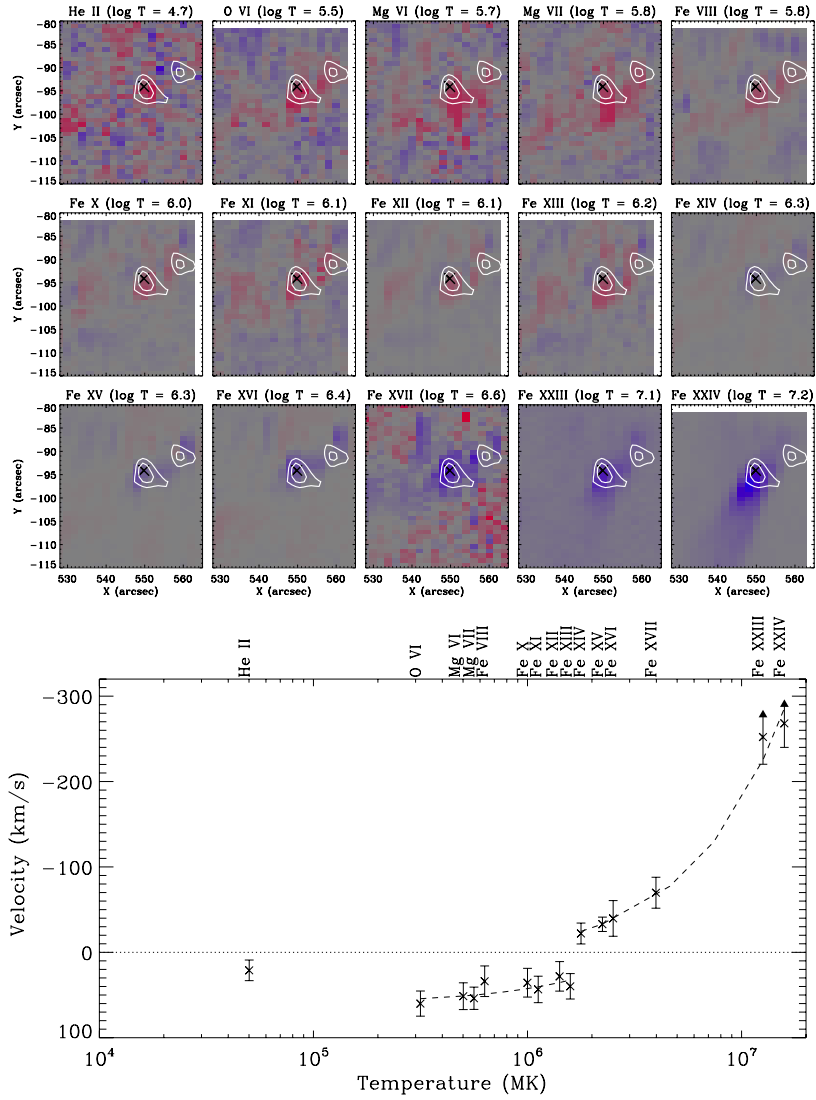


Figure 9. *Top*: Velocity maps in each line used for the observation ranging from 0.05 to 16 MK associated with the 2007 December 14 flare. Red/blue pixels denote downward/upward motions, respectively. The RHESSI 20–25 keV contours are overlaid. All velocity maps are scaled to ± 150 km/s. *Bottom*: Plasma velocity from a flare footpoint as a function of temperature for each of the emission lines. The dashed lines represent a weighted least-squares fit to the data points from 0.5 to 1.5 MK and 2.0 to 16 MK (Milligan & Dennis 2009). Copyright held by AAS.

During large flares, however, line profiles at footpoints become much more complicated. Associated with the 2006 December 13 flare, Imada et al. (2008) showed that the non-gaussian profiles derived from *Hinode*/EIS observation are varying with time during the flare. The line profiles are distorted very much. This means that a very complicated velocity field is formed inside flare loops.

6. Summary

We have quickly (and roughly) reviewed the dynamic phenomena observed at flares. It goes without saying that solar flares are very dynamic and are associated with many spectacular phenomena. Although the solar activity has been extremely low and very few large flares have been observed for these years, *Hinode* has undoubtedly shown the ability for the dynamic features of flares. There has been great development by recent observations, and we have some new findings from recent observations. However, there are still many unsolved questions, and they will be studied more. We now have many instruments both from ground-based and space-based, including STEREO and SDO. We are now awaiting new large flares.

Acknowledgments. AA wishes to thank Drs. H. Hara, H. Isobe and S. Takasao for their help to make figures in this manuscript. *Hinode* is a Japanese mission developed and launched by ISAS/JAXA, with NAOJ as domestic partner and NASA and STFC (UK) as international partners. It is operated by these agencies in co-operation with ESA and NSC (Norway).

References

- Antonucci, E., Gabriel, A. H., & Dennis, B. R. 1984, *ApJ*, 287, 917
 Asai, A., Hara, H., Watanabe, T., Imada, S., Sakao, T., Narukage, N., Culhane, J. L., & Doschek, G. A. 2008, *ApJ*, 685, 622
 Asai, A., Yokoyama, T., Shimojo, M., Kurokawa, H., & K., S. 2004a, *ApJ*, 611, 557
 Asai, A., Yokoyama, T., Shimojo, M., & Shibata, K. 2004b, *ApJL*, 605, 77
 Carmichael, H. 1964, in *The Physics of Solar Flares*, edited by W. N. Hess, NASA SP-50, 451
 Carrington, R. C. 1859, *MNRAS*, 20, 13
 Chen, P. F., Wu, S. T., Shibata, K., & Fang, C. 2002, *ApJL*, 572, 99
 Hara, H., Watanabe, T., Bone, L. A., Culhane, J. L., van Driel-Gesztelyi, L., & Young, P. R. 2009, in *The Second Hinode Science Meeting: Beyond Discovery-Toward Understanding*, edited by B. Lites, M. Cheung, T. Magara, J. Mariska, & K. Reeves (ASP), vol. 415 of ASP Conf. Ser., 459
 Hara, H., Watanabe, T., Matsuzaki, K., Harra, L. K., Culhane, J. L., Cargill, P., Mariska, J. T., & Doschek, G. A. 2008, *PASJ*, 60, 275
 Hirayama, T. 1974, *Sol. Phys.*, 34, 323
 Ichimoto, K., & Kurokawa, H. 1984, *Sol. Phys.*, 93, 105
 Imada, S., Hara, H., Watanabe, T., Asai, A., Kamio, S., Matsuzaki, K., Harra, L. K., & Mariska, J. T. 2008, *ApJL*, 679, 155
 Innes, D. E., Inhester, B., Axford, W. I., & Wilhelm, K. 1997, *Nature*, 386, 811
 Innes, D. E., McKenzie, D. E., & Wang, T.-J. 2003, *Sol. Phys.*, 217, 267
 Karlický, M., Fárník, F., & Mészáros, H. 2002, *A&A*, 395, 677
 Khan, J. I., & Aurass, H. 2002, *A&A*, 383, 1018
 Kopp, R. A., & Pneuman, G. W. 1976, *Sol. Phys.*, 50, 85
 Lin, J., Ko, Y.-K., Sui, L., Raymond, J. C., Stenborg, G. A., Jiang, Y., Zhao, S., & Mancuso, S. 2005, *ApJ*, 622, 1251
 McKenzie, D. E. 2000, *Sol. Phys.*, 195, 381

- McKenzie, D. E., & Hudson, H. S. 1999, *ApJL*, 519, 93
- Milligan, R. O., & Dennis, B. R. 2009, *ApJ*, 699, 968
- Moreton, G. E. 1960, *AJ*, 65, 494
- Narukage, N., Hudson, H. S., Morimoto, T., Akiyama, S., Kitai, R., Kurokawa, H., & Shibata, K. 2002, *ApJL*, 572, 109
- Narukage, N., & Shibata, K. 2006, *ApJ*, 647, 1122
- Nishizuka, N., Takasaki, H., Asai, A., & Shibata, K. 2010, *ApJ*, 711, 1062
- Ohyama, M., & Shibata, K. 1998, *ApJ*, 499, 934
- Parker, E. N. 1957, *JGR*, 62, 509
- Shibata, K. 1996, *Adv. Space Res.*, 17, 9
- 1997, in *Fifth SOHO Workshop: The Corona and Solar Wind Near Minimum Activity*, edited by A. Wilson, ESA SP-404, 103
- Shibata, K., & Tanuma, S. 2001, *Earth, Planets and Space*, 53, 473
- Sturrock, P. A. 1966, *Nature*, 211, 695
- Sweet, P. A. 1958, in *Electromagnetic Phenomena in Cosmical Physics*, edited by B. Lehnert (Cambridge: Cambridge University Press), vol. 6 of *IAU Symp.*, 123
- Thompson, B. J., Reynolds, B., Aurass, H., Gopalswamy, N., Gurman, J. B., Hudson, H. S., Martin, S. F., & Cyr, O. C. S. 2000, *Sol. Phys.*, 193, 161
- Uchida, Y. 1968, *Sol. Phys.*, 4, 30
- Wang, T., Sui, L., & Qiu, J. 2007, *ApJL*, 661, 207
- Yokoyama, T., Akita, K., Morimoto, T., Inoue, K., & Newmark, J. 2001, *ApJL*, 546, 69